RESEARCH PAPER

Reduction in liquid metal embrittlement cracking using weld current ramping

Christopher DiGiovanni[1] (ORCID) · S. Bag[2] · C. Mehling[1] · K. W. Choi[1] · A. Macwan[3] · E. Biro[1] · N. Y. Zhou[1]

Abstract

Advanced high-strength steels (AHSS) used in automotive structural components are commonly protected from corrosion using zinc coatings. However, the steel/zinc system creates the potential for liquid metal embrittlement (LME) during welding. Although adjustments to the welding process have been studied, the present literature has not examined the use of variable input currents for LME reduction. In this work, a ramp down welding current showed LME severity decreased by 60% compared to a standard constant current. Reductions in both crack size and number of cracks were observed for high currents ($I_{max} + 20\%$). A numerical model of the resistance spot welding process was constructed, which showed when welding with a ramp down welding current, the electrode-to-sheet interface spends less time at an LME-sensitive temperature compared to the standard welding current. Furthermore, it avoids a large jump in tensile stress when the electrodes are removed.

Keywords Liquid metal embrittlement · Resistance spot welding · Advanced high-strength steel · Variable input current · Thermal modelling · Finite element analysis

1 Introduction

In recent years, environmental concerns about carbon emissions and fossil fuel usage led to regulations for lower vehicle fuel consumption, requiring automotive manufacturers to improve vehicle fuel efficiency to reduce climate change and damage [1–4]. The industry looks to achieve this by reducing vehicle weight; however, mechanical performance of the materials and structures cannot be compromised. This has led to the development of advanced high-strength steels (AHSS) which have higher strength, allowing parts to be made from thinner sheets, and have been increasingly implemented in automotive body-in-

white structures [5–7]. In addition, AHSS are protected from the corrosive environment by a zinc coating. A thin layer of zinc provides cathodic protection to the underlying AHSS substrate.

The most common joining process associated with automotive assembly is resistance spot welding (RSW). RSW functions by passing a high current through a lap joint to generate heat. Heat is concentrated at the sheet-to-sheet interface, due to its high contact resistance, and a volume of metal is melted during the weld time. During the proceeding hold time, the weld nugget is solidified under the force and cooling of the electrodes [8, 9]. However, the addition of the zinc coating adds complexities to the welding process, such as liquid metal embrittlement (LME) [10, 11]. Zinc melts at 419 °C, far below the melting point of the steel substrate (~ 1475 °C). During welding, the liquid zinc penetrates into AHSS grain boundaries, which are under tensile stresses from the RSW process; this allows LME cracks to open and propagate during RSW [12–14]. Studies have shown LME is innocuous [15, 16]; however, recent work has shown that in extreme cases LME may lead to a decrease in joint strength [17, 18].

For LME to occur there are three necessary factors that must be present: liquid zinc in direct contact with solid steel, a susceptible microstructure, and tensile stresses [19, 20]. The point at which zinc is in a liquid state and tensile stresses are present is governed by the welding process. Therefore, the welding

---

✉ Christopher DiGiovanni
ctdigiov@uwaterloo.ca

1 Department of Mechanical and Mechatronics Engineering, University of Waterloo, Waterloo, Canada

2 Department of Mechanical Engineering, Indian Institute of Technology Guwahati, Guwahati, Assam, India

3 ArcelorMittal Global Research, ArcelorMittal Dofasco, Hamilton, Canada

Table 1 Material examined

Steel	Main alloying elements (wt.%)					
TRIP1100	C	Mn	Si	Cr	Al	Mo
	0.20	2.17	1.61	0.03	–	–
	Mechanical properties					
	Thickness (mm)	Yield strength (MPa)	Tensile strength (MPa)	% elongation	Top coating thickness (g/m^2)	Bottom coating thickness (g/m^2)
	1.6	861	1100	14.6	58	70

parameters have a large influence on LME crack formation during RSW. Previous work carried out by Beal et al. suggested the modification of the RSW process parameters to avoid activating LME [14]. However, it is currently unclear which process parameters lead to severe LME cracking. A recent study by Choi et al. found that the instant the electrodes are released, large tensile stress developed due to the sudden change in cooling rate [21]. Choi et al.'s study implies the management of the cooling rate discontinuity can result in decreased LME severity. If the weld surface is much cooler, then the cooling rate will naturally decrease to a point where the shock from the electrode removal will not be as drastic.

Several attempts have been made to adjust the welding schedule to reduce LME severity, including increasing electrode force [22], use of pre-current [19], and using multi-pulse weld schedules with different lengths [23, 24]. In each of these studies, changes in the LME crack population were attributed to changes in the thermal profile at the location of LME cracks. However, each of these studies used a rectangular shape or constant input current. Sloped or ramping input currents have been used in several other applications [25–27] but have not yet been applied to LME reduction during RSW. The present study explores the use of a negatively sloped or ramp down input current to start cooling the weld earlier in the cycle, mitigating the thermal discontinuity at the electrode release. This will bring the thermal cycle into an LME free region without increasing the overall cycle time. The effects using a standard constant current or a ramp down current on LME crack severity was compared using a TRIP1100 AHSS

joints. LME cracking in each sample type was quantified and evaluated, showing major differences. In addition, a finite element analysis (FEA) model was constructed of the welding process to understand the contrasts in the temperature and stress profiles during the welding process.

2 Materials and methods

2.1 Materials

This study was carried out on a transformation induced plasticity steel with a tensile strength of 1100 MPa (TRIP1100). As the name suggests, during plastic deformation the retained austenite in the microstructure transforms to martensite, which provides excellent strain hardening. The material was donated by the International Zinc Association, as it is highly susceptible to LME and is of interest to industry. The chemical composition and mechanical properties can be found in Table 1.

2.2 Welding schedules

Resistance spot welding was completed using a trans-gun direct current spot welding machine mounted on a 6-axis robot arm. The electrode gun is C type clamp gun with servo-controlled electrode force and Rexroth welding controller. In the standard condition, a two equal pulse welding scheme was used as recommended by American Welding Society D8.9 specification for this material grade [28]. The

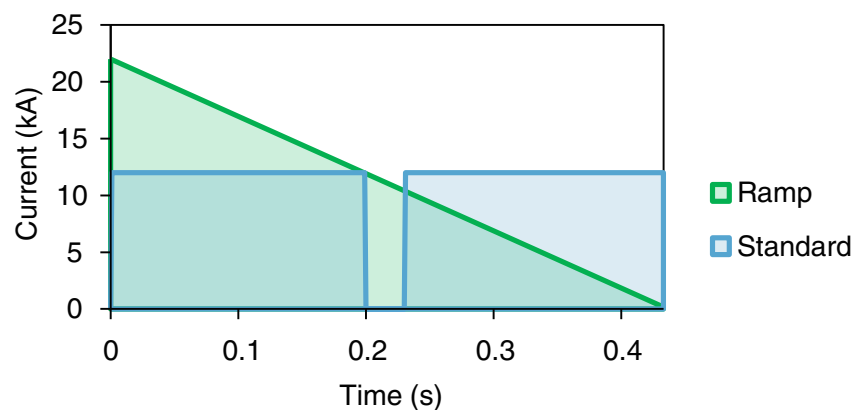**Fig. 1** Current schemes for the standard and ramp conditions

Table 2 Welding schedules for the standard the ramp current conditions

Welding schedule	Welding current (kA)	Electrode dia. (mm)	Welding time (ms)	Hold time (ms)	Force (kN)
Standard	12	7.0	200–33–200	167	3.5
Ramp	Equation 2	7.0	433	167	3.5

ramping current condition was designed to give a weld nugget of the same size. To do this, the input current was designed to best match the heat input of the standard condition. In order to keep the process heat input the same, the area under both conditions' current-time graph was kept approximately constant. This is shown mathematically in Eq. 1, which was used to determine the ramp peak current and the slope of the ramp line.

$$\int_0^{t_f} I_S(t)dt \approx \int_0^{t_f} I_R(t)dt \tag{1}$$

where I_S is the current of the standard scheme, $I_R(t)$ is the current of the ramping scheme, and t_f is the total weld time. If we assume that $I_R(t_f) = 0$, Eq. 1 can be simplified to

$$\int_0^t I_S(t)dt \approx \frac{1}{2} I_{Ri} t_f$$

where I_{Ri} is the peak current or the current at $t = 0$. For the standard case, a current well above the expulsion current (I_{max}) for this material grade was selected. Using $I_{max} + 20\%$ (12 kA) will provide the most severe case of LME and will allow for an obvious study of LME reduction. Using $I_S = 12 kA$ and from Fig. 1 and Eq. 1, the ramp down current was determined and is defined in Eq. 2. With the current profile of the ramp case determined samples were welded under both conditions. The entire welding schedule is summarized in Table 2.

$$I_R = -50.4(t) + 22 \tag{2}$$

After welding, the coupons were cross-sectioned along their width (direction perpendicular to the long axis of the coupon) using a precision saw, then hot-mounted, ground, and polished for a mirror finish. The samples were examined for LME cracks using an optical microscope. Crack depth in the thickness direction was measured using the ImageJ® software and the data was compiled into the lognormal median crack depth, the mean number of cracks per sample, and the LME cracking index. The LME cracking index was developed to holistically quantify LME crack [29]. The LME crack index is defined in Eq. 3

$$CI = \frac{nL}{\tau} \tag{3}$$

where n is the mean number of cracks per samples, L is the lognormal median crack depth, and τ is the sheet thickness.

2.3 Theoretical model construction

A three-dimensional thermo-mechanical model of the welding process was made using the *Abaqus FEA* software. To save computational power and since the model is of planar symmetry, a quarter model was used as shown in Fig. 2. A suitable mesh size of ~ 2000 hexahedral full integration elements was used as it gave an optimal balance of accuracy and computational demands.

2.3.1 Thermal model

The thermal model was constructed in accordance with the experimental RSW parameters shown in Table 2. A schematic of the heat input locations is shown in Fig. 2.

Figure 2 shows the three sources of heat generation. These are the sheet-to-sheet contact resistance heating, modelled as a surface heat flux (Q_{C1} [W/m^2]); the electrode-to-sheet contact resistance heating, modelled as a surface heat flux (Q_{C2} [W/m^2]); and the bulk material heating, which was modelled as a volumetric heat flux (Q_b [W/m^3]). The contact resistance during the RSW process is a complex phenomenon; however, there are several established mathematical models in the field [30]. For this study, a popular contact resistance model for RSW proposed by Greitmann and Rother was employed
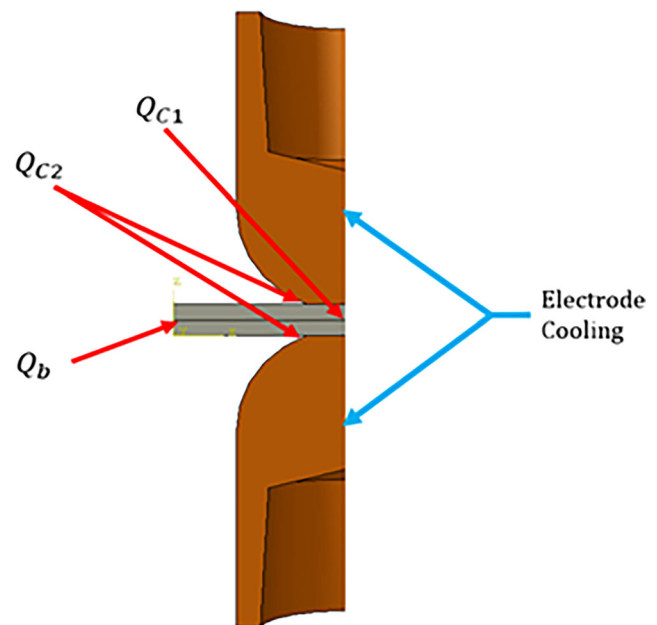

Fig. 2 Thermal model set up; locations of heat generation and cooling

during the thermal calculations [31]. Cooling is also present in the form of an idealized thermal contact to the water-chilled electrodes. The model was designed so that at the end of the weld cycle, the electrodes are removed from contact. Temperature-dependant material properties were also accounted for.

2.3.2 Mechanical boundary conditions

The results from the thermal model were transferred to the thermo-mechanical model, which has the addition of the mechanical boundary conditions. The electrodes apply a force equal to what was used in the experimental work. A mechanical contact condition is applied at the sheet-to-sheet and electrode-to-sheet interfaces to allow for deformation of the surfaces in contact. Similar to the thermal model, once the hold time is complete, the electrode force is deactivated.

3 Results and discussions

3.1 Standard current samples

The results of the standard current showed detrimental amounts of LME cracking. LME cracks were observed across the weld surface in both the electrode indent area and in the weld shoulder. An image showing a typical cross-section of the standard current type sample is shown in Fig. 3.

It can clearly be seen from Fig. 3 that the standard current is a case of severe LME cracking. Large LME cracks were observed in several locations. However, to fully quantify LME severity, the cracks were counted, measured, and are presented as the crack index, lognormal median crack depth and mean number of cracks per sample in Table 3 with a 95% confidence interval. The high values for crack depth and number of cracks results in a high cracking index which indicates poor weld quality [29]. A weld with LME cracks this severe is not acceptable and must be remedied.

However, in order to develop an effective mitigation technique, the crack development mechanism must be understood.

Table 3 LME severity metrics for the standard current scheme showing a large crack index

LME severity	Cracking index	Lognormal median crack depth (μm)	Mean number of cracks
Value	1.74	159.4	17.4
95% confidence interval	± 0.07	± 3.1	± 2.5

The temperature and stress profiles during the welding process can offer insight into the formation of LME cracks during welding.

3.2 Thermo-mechanical modelling

The theoretical model results give some understanding of the thermal and mechanical behaviour of the steel sheets during the welding process. Before the analysis of the welding cycle, the nugget predicted by the model was compared to an experimental cross-section. The thermal model results show an acceptable degree of accuracy in terms of predicting temperature fields. Figure 4 shows the temperature field at the end of the weld time. The liquid AHSS steel region is shown in grey, which matches the shape and size of the experimentally measured nugget with reasonable accuracy.

The regions where LME is active are of interest when examining the temperature and stress profiles. The LME active region has previously been characterized as the area where zinc is liquid and stresses are tensile [21, 22]. The temperature and maximum principle stress plots of the centre electrode indent area for the standard current scheme are shown in Fig. 5, and the LME active regions have been highlighted on the stress plot. From the temperature profile, the surface spends most of its time above the zinc melting temperature. However, during this time frame, the stresses are mostly compressive. It is well documented that the stresses during the heating cycle of RSW are dominated by compression in the electrode indent region [9, 32]; however, tensile stresses are required for LME cracks to form. Tensile stresses start to build upon cooling, but there is a clear overlap of liquid zinc and high tensile stresses when the

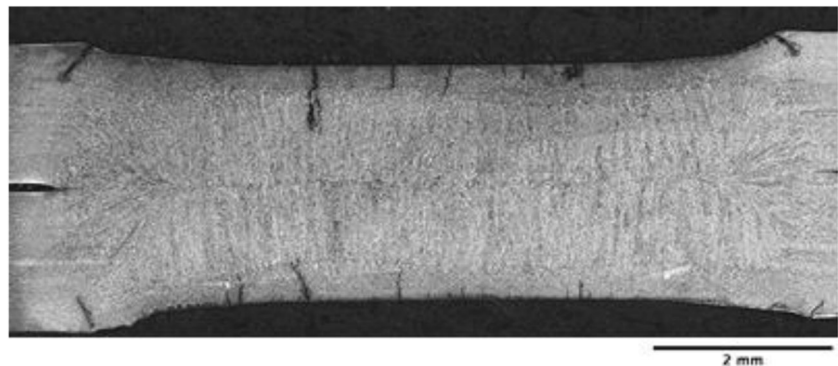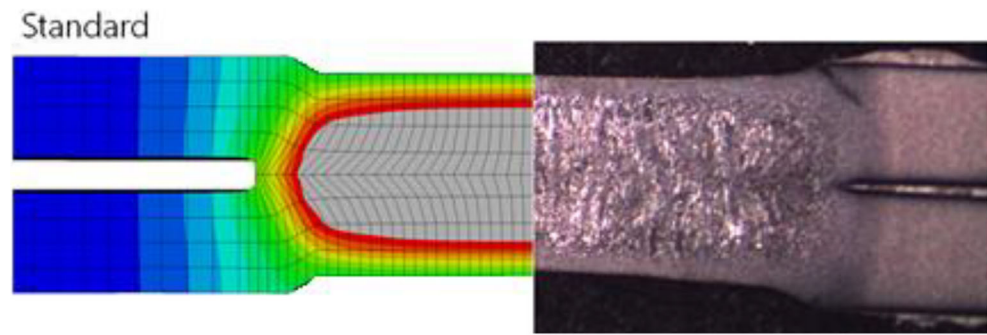**Fig. 3** Typical weld cross-section of the standard welding current

2 mm

electrodes are released ($t > 0.6$). Therefore, it is thought that the LME cracks observed in the weld centre area form after the heating cycle and once the nugget was solidified.

The detected issue with the standard current is a sudden increase in tensile stresses while still in the LME active region. Thus, the removal of one or both factors will lead to a decrease in LME cracking. One approach is to use a negatively sloped or ramp down current. If cooling starts earlier, the surface temperature will be below the zinc melting temperature sooner and the zinc will have solidified by the time the electrodes release. Furthermore, the reduction in overall heat in the two sheets upon electrode release will lead to less thermal shock at the surfaces when the heat sink is removed. The use of a ramp down current will theoretically result in less tensile stresses and liquid zinc when the electrodes are released.

To maximize this effect, current was ramped down through the entirety of the welding cycle. Using the same model set-up, another simulation was run with a ramp down current to produce a nugget of a similar size. The simulation results of the surface temperature and stress profiles are shown and compared against the standard current profiles in Fig. 6. The plots show the temperature and stress metrics for the centre location of the electrode indent. From the temperature plots, the thermal cycle for each case is different. The ramp down current case begins cooling much sooner than the standard current case. This allows the ramp down current case to spend less time above the zinc melting temperature, particularly when the electrodes release. This potentially limits opportunity for LME cracks to form. However, the ramp down current reaches a higher peak temperature, early in the welding cycle.

When examining the corresponding stress plots (Fig. 6), it is true that the initial peak temperature will not contribute to LME since the stresses are compressive. In contrast to the standard constant current, the ramp down current case does not experience a jump in tensile stress at the instant of electrode release. This is likely due to less heat being conducted from the thickness centre of the weld to the weld surface, which is reflected by the lesser increase in temperature at this point.

In addition to the electrode indent area, the weld shoulder region is also of interest since LME cracks have commonly been observed there [33]. The temperature and stress plots for a location in the shoulder area are shown in Fig. 7. The LME active regions are highlighted on the stress plot. Like the electrode indent area, the ramp down current case reaches a higher peak temperature, but otherwise, the temperature profiles for both current cases follow the same trends in this location. They are both observed to reach a peak temperature early in the welding cycle. The shoulder area in both cases is initially in tension as the electrode pushes into the material. Then the area goes into compression as area cools on contact with the electrode. Towards the end of the welding cycle, the area is put under tension as the weld area cools. These results show the major difference between the two cases regarding shoulder cracks is the ramp down case spending less time in the LME active region.

Fig. 5 Temperature and stress plots for the standard constant current case on the weld surface in the electrode indent area
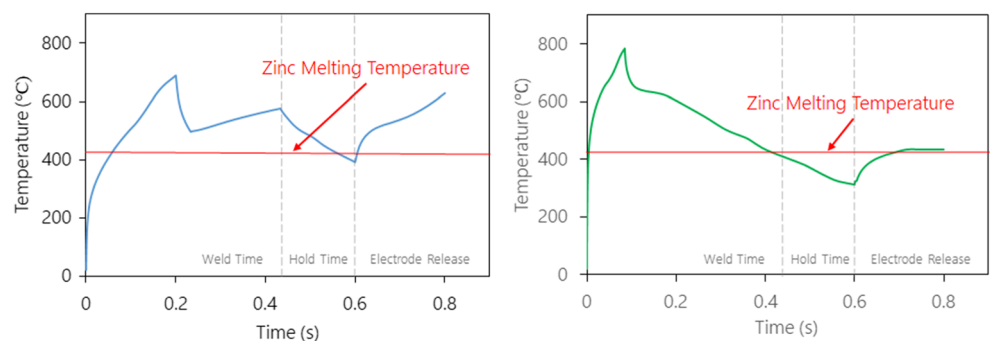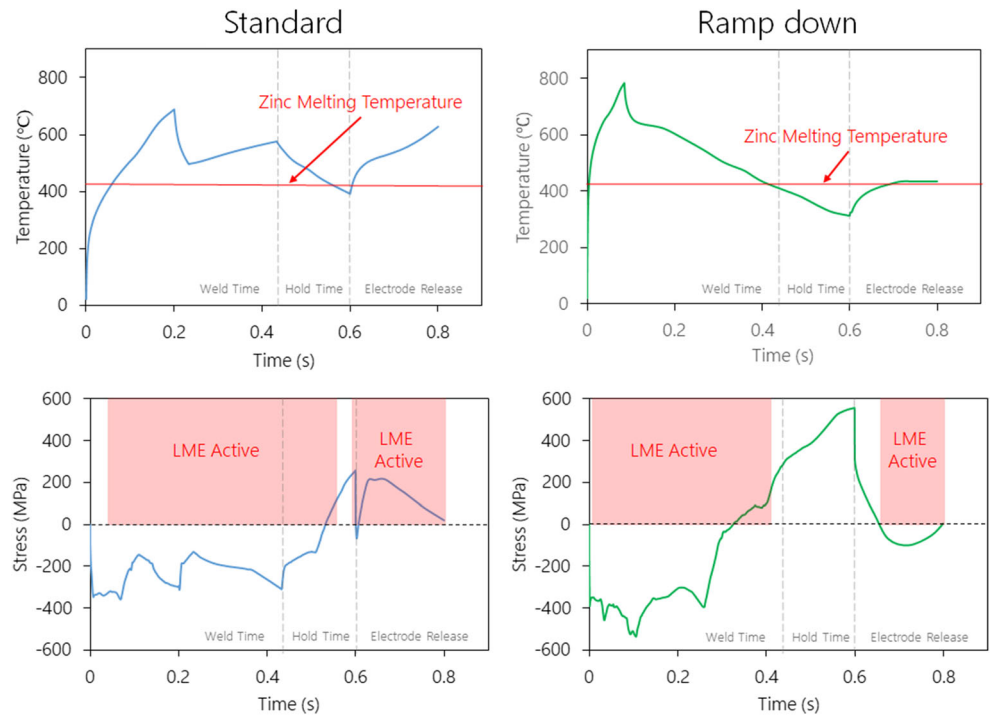
From the results of the thermo-mechanical model, there is expected to be a decrease in LME crack severity in the ramp down current case, particularly for electrode indent area cracks. The ramp down current case does not experience the large tensile stress increase in the indented area when the electrodes are released. However, it is unclear whether there will be a difference in the development of LME shoulder cracks. LME shoulder cracks are expected in both cases, but perhaps less frequent in the ramp down current case due to less time in the LME active region. To determine if the variable current input made a practical difference on LME crack development, the experimental ramp down LME evidence must be examined.
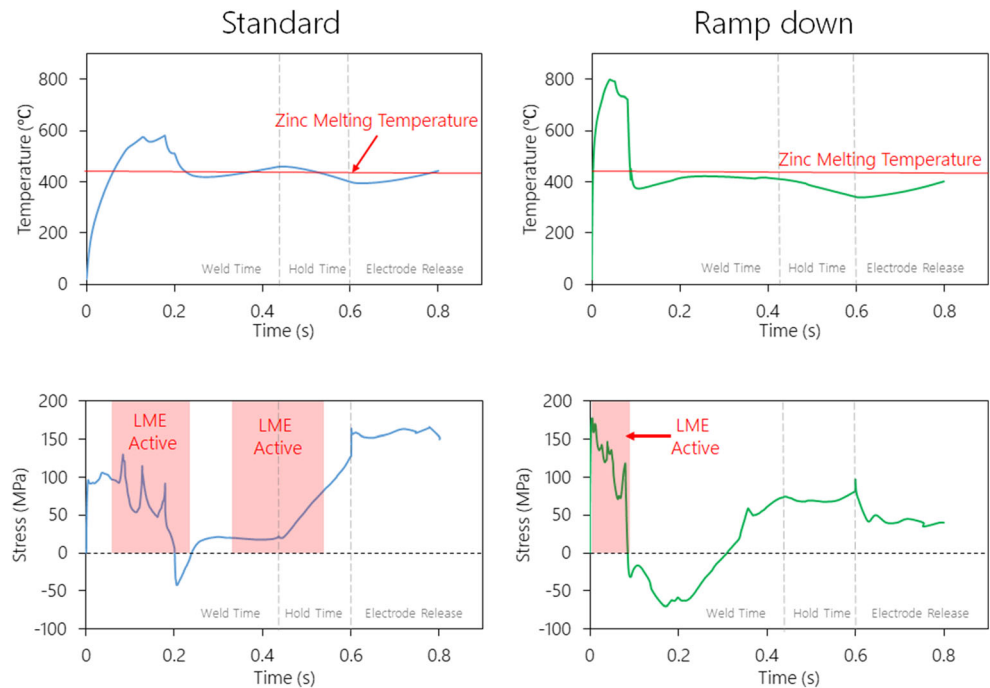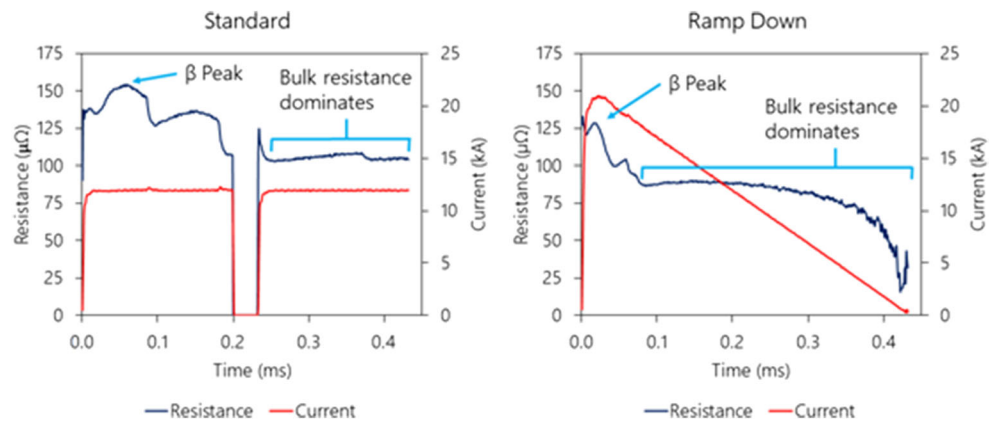
Fig. 8 Current and resistance monitoring for standard constant current welding schedule and ramp down current schedule

## 3.3 Ramp down current and liquid metal embrittlement reduction

The results of the different welding schedules yield very similar weld geometries. The final weld nugget size is expected to be similar, since a similar heat input was used for both welding schedules. Statistical analysis showed there to be no significant difference in nugget size between the two sample types and had a mean nugget size of 7.7 ± 0.4 mm. Despite the similar final nugget geometry, the two conditions underwent different heating cycles due to the difference in the input current waveform. The current and resistance monitoring from the welding controller are shown in Fig. 8.

From Fig. 8, the contact resistance decreases and material bulk resistance dominates much sooner in the ramp schedule relative to the standard schedule. The first resistance peak after

the inflexion point is labelled as the β peak, which indicates the start of nugget growth [34]. The ramp down current experiences the β peak much sooner, implying that melting at the sheet-to-sheet interface happened earlier. Furthermore, the β peak value is lower when welding with the ramp down schedule compared to the standard constant current schedule. This is likely due to the use of a higher current at the time the respective β peak occurs. Overall, there is a much larger heat build-up in the initial portion of the ramp current case, whereas for the standard case, heat is generated consistently throughout the cycle.

A comparison of typical cross-sections for each sample type and the local cracking index on cross-section regions is shown in Fig. 9. The figure shows a stark difference in LME cracking between the ramp down and standard cases. The ramp down current contains fewer LME cracks, particularly

Fig. 9 Comparison of LME cracks in welded cross-sections of standard weld type and ramping current and a contour map showing the cracking index at different locations
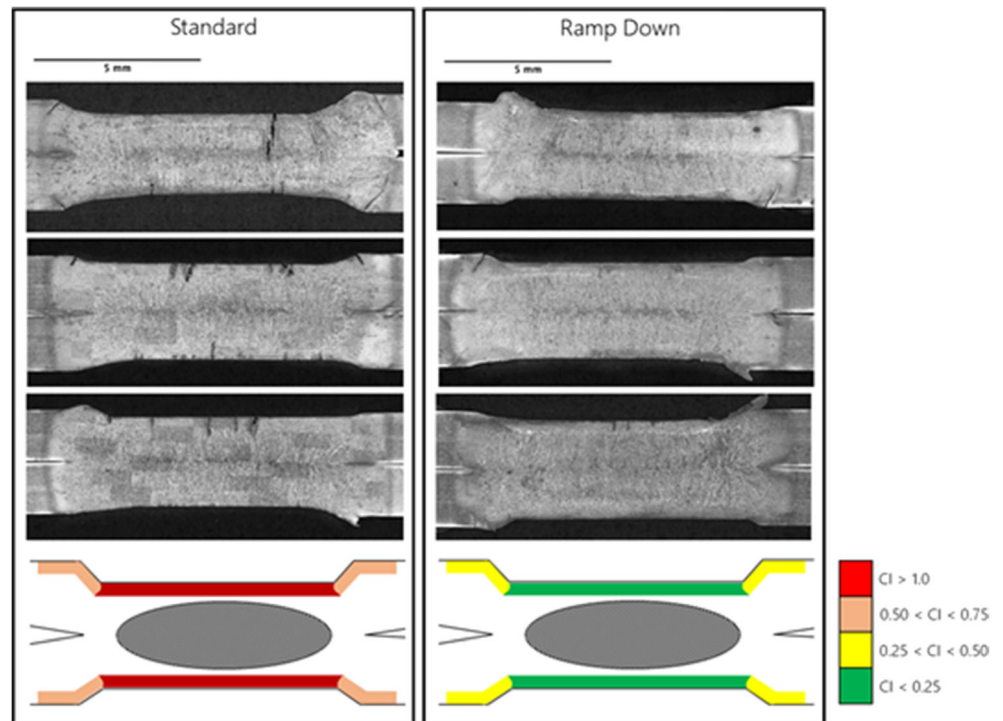
in the centre. It has been shown from the FEA process model that the centre weld surface in the ramp down case spends less time in the LME active region and mitigates the tensile stresses upon electrode removal. This results in fewer cracks forming in this location, which also do not propagate as far as in the constant current case. It is also interesting to note that in the standard constant current case, the large cracks propagate into the weld nugget, meaning they grew after the nugget was solidified. This agrees with the FEA model results which showed high tensile stresses on the electrode indent surface after solidification of the nugget. Additionally, shoulder LME cracks were observed to be less frequent in the ramp down current case, albeit similar in size in both cases. This is described by the model results, which showed the ramp down current spent less time in the LME region, resulting in less opportunity for LME cracks to form. However, cracks that formed experienced similar stress levels and grew similar in size to the standard case.

In order to fully characterize the LME crack populations, a full analysis of LME crack metrics was carried out. The results for ramp current cracking index with a 95% confidence interval are compared against the standard current in Fig. 10.

From the LME crack index shown in Fig. 10, there is clearly a reduction in LME crack severity at $I_{max} + 20\%$. This is particularly seen when examining the overall LME cracking index, where a 60% decrease is observed. Furthermore, for the lognormal median crack depth and mean number of cracks a 32% and 41% decrease respectively was found. Finally, the maximum crack depth in the standard case (1319 μm) was significantly larger compared to the ramp down maximum crack depth (597 μm). Generally, these results show that LME is less severe when using a ramp down current as opposed to the standard constant input current.

The large reduction in the number of cracks and crack depth leads to a decrease in overall crack severity since large cracks are less likely to form in critical locations [18, 29]. The ramp down methodology was further applied to the I_{max} heat input case and showed a similar trend. The cracking index was reduced 0.39 with a more noticeable reduction in shoulder
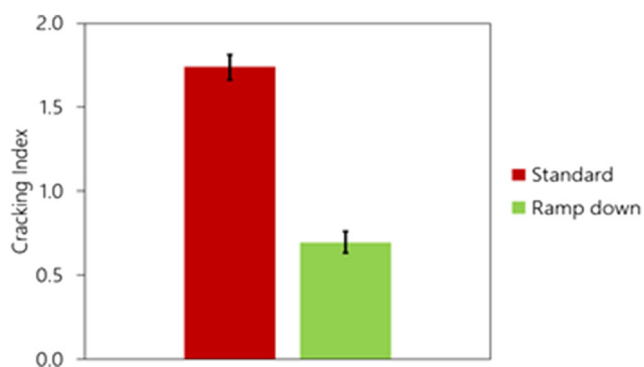

Fig. 10 Crack index for ramp down current compared to standard constant current at $I_{max} + 20\%$

crack severity. Therefore, it has been shown that highly LME susceptible AHSS can be welded with typical heat inputs without concern for joint strength loss and severe cracking. The use of a ramp down current shows promising results and is only one of several approaches to temperature and stress management for LME mitigation during RSW.

4 Conclusion

The use of a ramp down current led to reduced LME cracking in the form of decreased lognormal median crack depth (159.4 μm reduced to 109.0 μm) and fewer average cracks per sample (17.4 reduced to 10.2). Compared to the standard constant current scheme, the ramp down current weld surface's temperature profile spent less time in the liquid zinc region while under tension leading to less opportunity for LME cracks to form. In addition, the ramp down current scheme did not undergo a sudden increase in tensile stresses at the weld surface when the electrodes were released. Furthermore, it should be noted that these results are for an extreme case of heat input ($I_{max} + 20\%$); when the ramp down methodology was applied to typical heat inputs (I_{max}), a similar reduction trend was observed. Overall, it was shown that variable input currents can be utilized for LME reduction during RSW and that process temperature and stress management is an effective technique for LME mitigation.

References

1. Cooper AI (2015) Materials chemistry: cooperative carbon capture. Nature 519:295
2. Jakob M, Hilaire J (2015) Unburnable fossil-fuel reserves. Nature 517:150–151. https://doi.org/10.1038/517150a
3. McNutt M (2013) Climate change impacts. Science 341:435. https://doi.org/10.1126/science.1243256
4. Creutzig BF, Jochem P, Edelenbosch OY et al (2015) Transport: a roadblock to climate change mitigation? Science (80-) 350:911–912. https://doi.org/10.1126/science.aac8033
5. Parkes D, Westerbaan D, Nayak SS, Zhou Y, Goodwin F, Bhole S, Chen DL (2014) Tensile properties of fiber laser welded joints of high strength low alloy and dual-phase steels at warm and low temperatures. Mater Des 56:193–199. https://doi.org/10.1016/j.matdes.2013.10.087
6. Parkes D, Xu W, Westerbaan D, Nayak SS, Zhou Y, Goodwin F, Bhole S, Chen DL (2013) Microstructure and fatigue properties of fiber laser welded dissimilar joints between high strength low alloy and dual-phase steels. Mater Des 51:665–675. https://doi.org/10.1016/j.matdes.2013.04.076
7. Xu W, Westerbaan D, Nayak SS, Chen DL, Goodwin F, Zhou Y (2013) Tensile and fatigue properties of fiber laser welded high strength low alloy and DP980 dual-phase steel joints. Mater Des 43:373–383. https://doi.org/10.1016/j.matdes.2012.07.017
8. Kimchi M, Phillips DH (2017) Resistance spot welding, fundamentals and applications for the automotive industry. Columbus, Ohio

9. Zhang H, Senkara J (2012) Resistance welding: fundamentals and applications

10. Kim YG, Kim IJ, Kim JS, Chung YI, Choi DY (2014) Evaluation of surface crack in resistance spot welds of Zn-coated steel. Mater Trans 55:171–175

11. Jiang C, Thompson a. K, Shi MF, et al (2003) Liquid metal embrittlement in resistance spot welds of AHSS steels. In: AWS Professional Program. p 9A

12. Ina K, Koizumi H (2004) Penetration of liquid metals into solid metals and liquid metal embrittlement. Mater Sci Eng A 387–389: 390–394. https://doi.org/10.1016/j.msea.2004.05.042

13. Joseph B, Barbier F, Dagoury G, Aucouturier M (1998) Rapid penetration of liquid Bi along Cu grain boundaries. Scr Mater 39: 775–781. https://doi.org/10.1016/S1359-6462(98)00230-9

14. Beal C, Kleber X, Fabregue D, Bouzekri M (2012) Embrittlement of a zinc coated high manganese TWIP steel. Mater Sci Eng A 543: 76–83. https://doi.org/10.1016/j.msea.2012.02.049

15. Benlatreche Y, Ghassemi-Armaki H, Duchet M, et al (2017) Spot-weld integrity of Zn-coated 3rd gen. Advanced high strength steel in presence of LME. In: International Automotive Body Congress (IABC 2017 Dearborn). pp 9–18

16. Benlatreche Y, Duchet M, Dupuy T, Cornette G Effect of liquid metal embrittlement cracks on the mechanical performances of spot welds. In: 5th International Conference on Steels in Cars and Trucks. Amsterdam

17. DiGiovanni C, Biro E, Zhou NY (2018) Impact of liquid metal embrittlement cracks on resistance spot weld static strength. Sci Technol Weld Join 0:1–7. https://doi.org/10.1080/13621718.2018.1518363

18. DiGiovanni C, Han X, Powell A, Biro E, Zhou NY (2019) Experimental and numerical analysis of liquid metal embrittlement crack location. J Mater Eng Perform 28:2045–2052. https://doi.org/10.1007/s11665-019-04005-2

19. Kim YG, Kim IJ, Kim JS et al (2014) Evaluation of surface crack in resistance spot welds of Zn-coated steel. Japan Inst Met Mater 55: 171–175. https://doi.org/10.2320/matertrans.M2013244

20. Ashiri R, Haque MA, Ji C-W, shamanian M, Salimijazi HR, Park YD (2015) Supercritical area and critical nugget diameter for liquid metal embrittlement of Zn-coated twining induced plasticity steels. Scr Mater 109:6–10. https://doi.org/10.1016/j.scriptamat.2015.07.006

21. Choi D, Sharma A, Jung JP (2018) Parametric study for liquid metal embrittlement in. In: Sheet Metal Welding Conference XVIII. American Welding Society, Livonia, MI, pp 1–9

22. Choi DY, Sharma A, Uhm SH, Jung JP (2018) Liquid metal embrittlement of resistance spot welded 1180 TRIP steel: effect of electrode force on cracking behavior. Met Mater Int 25:219–228. https://doi.org/10.1007/s12540-018-0180-x

23. Wintjes E, Macwan A, Biro E, Zhou YN (2018) Effect of multi-pulse welding on LME severity in RSW joints. Sheet Met Weld Conf XVIII

24. Ashiri R, Shamanian M, Salimijazi HR, Haque MA, Bae JH, Ji CW, Chin KG, Park YD (2016) Liquid metal embrittlement-free welds of Zn-coated twinning induced plasticity steels. Scr Mater 114:41–47. https://doi.org/10.1016/j.scriptamat.2015.11.027

25. Xu J, Zhai T (2008) The small-scale resistance spot welding of refractory alloy 50Mo-50Re thin sheet. Jom 60:80–83. https://doi.org/10.1007/s11837-008-0096-x

26. Kaars J, Mayr P, Koppe K (2016) Generalized dynamic transition resistance in spot welding of aluminized 22MnB5. Mater Des 106: 139–145. https://doi.org/10.1016/j.matdes.2016.05.097

27. Soundarrajan M, Pasupathi K, Srinivasan N, Vengatesh MP (2015) Experimental investigation of resistance spot welding of duplex stainless steel experimental investigation of resistance spot welding of duplex stainless steel. Int J Appl Eng Res

28. American Welding Society (2012) American Welding Society: test method for evaluating the resistance spot welding behavior of automotive sheet steel materials (AWS D 8.9M). 1–107

29. Wintjes E, DiGiovanni C, He L, et al (2019) Quantifying the link between crack distribution and resistance spot weld strength reduction in liquid metal embrittlement susceptible steels. Weld World

30. Hamedi M, Atashparva M (2017) A review of electrical contact resistance modeling in resistance spot welding. Weld World 61: 269–290. https://doi.org/10.1007/s40194-016-0419-4

31. Greitmann MJ, Rother K (1998) Numerical simulation of the resistance spot welding process using spotwelder. In: Cerjak H, Bhadeshia HKDH (eds) Mathematical modelling of weld phenomena 4. pp 531–544

32. Nied H (1984) The finite element modeling of the resistance spot welding process. Annu AWS Conv:123–133

33. Bhattacharya D (2018) Liquid metal embrittlement during resistance spot welding of Zn-coated high-strength steels. Mater Sci Technol 34:1809–1829. https://doi.org/10.1080/02670836.2018.1461595

34. Dickinson DW, Frankling JE, Stanya A (1980) Characterization of spot welding behavior by dynamic electrical parameter monitoring. Weld J